Plant, Cell & Environment

Plant, Cell and Environment (2015) **38**, 2035–2047 doi: 10.1111/pce.12528

Original Article

Light-harvesting superstructures of green plant chloroplasts lacking photosystems

Erica Belgio, Petra Ungerer & Alexander V. Ruban

School of Biological and Chemical Sciences, Queen Mary University of London, London E1 4NS, UK

ABSTRACT

The light-harvesting antenna of higher plant photosystem II (LHCII) is the major photosynthetic membrane component encoded by an entire family of homologous nuclear genes. On the contrary, the great majority of proteins of photosystems and electron transport components are encoded by the chloroplast genome. In this work, we succeeded in gradually inhibiting the expression of the chloroplast genes that led to the disappearance of the photosystem complexes, mimicking almost total photoinhibition. The treated plants, despite displaying only some early signs of senescence, sustained their metabolism and growth for several weeks. The only major remaining membrane component was LHCII antenna that formed superstructures – stacks of dozens of thylakoids or supergrana. Freeze-fracture electron microscopy revealed specific organization, directly displaying frequently bifurcated membranes with reduced or totally absent photosystem II (PSII) reaction centre complexes. Our findings show that it is possible to accumulate large amounts of light-harvesting membranes, organized into three-dimensional structures, in the absence of reaction centre complexes. This points to the reciprocal role of LHCII and PSII in self-assembly of the three-dimensional matrix of the photosynthetic membrane, dictating its size and flexible adaptation to the light environment.

Key-words: electron microscopy; grana; LHCII; NPQ; photoinhibition; photosystem II.

Abbreviations: ΔpH, proton gradient; CEF, cyclic electron flow; DAD, 2,3,5,6-tetramethyl-phenylenediamine; DCMU, 3-(3,4-dichlorophenyl)-1,1-dimethylurea; EM, electron microscopy; FPLC, fast protein liquid chromatography; F_v/F_m, quantum yield of PSII; LED, light-emitting diode; LHCII, light-harvesting complex of photosystem II; NPQ, non-photochemical quenching; PAM, pulse amplitude modulated fluorimetry; PSII, photosystem II; RCII, reaction centre of PSII.

INTRODUCTION

Photosynthetic light harvesting is a crucial process that occurs in the antenna complexes of the photosynthetic membrane capable of increasing the photon capture efficiency by the reaction centres up to 300 times (Ruban 2012). The size of the photosynthetic antenna can be adjusted during the process of acclimation to environmental light intensity (Anderson *et al*. 1988; Anderson & Osmond 2001). However, exposure to high light intensities can cause a breakdown of the photosynthetic reaction centres (most noticeably those of the photosystem II, RCII) leading to the decrease in their concentration relative to the concentration of light-harvesting complexes. This process is called photoinhibition (Powles 1984; Barber 1995) since it reflects the sustained decline of the photosynthetic efficiency. However, not much is known about the effect of depletion from the reaction centre complexes of photosystems in the course of acute photoinhibition on the structure and functions of the photosynthetic membrane. In addition, the question, to what extent this decline affects plant growth, productivity and well-being, remains controversial (Baker & Bowyer 1994). General energy balance considerations, as well as empirical studies, predicted a linear relationship between the amount of captured light energy and dry mass as well as productivity of the crop canopy (Baker & Bowyer 1994). Other reports expressed doubts that naturally occurring photoinhibition could significantly undermine plant productivity in the long run (Ögren 1994). The cause of such controversy may lie in the combination of various environmental factors (other than light) superimposed upon the developmental stages of the plant life cycle. In this study, we watered plants with low concentrations of an inhibitor of plastid ribosomes, the antibiotic lincomycin, in order to inhibit formation of photosystems (Denslow & O'Brien 1974; Mulo *et al*. 2003; Bachmann *et al*. 2004). Lincomycin was chosen because, in contrast to chloramphenicol, it was shown not to prevent translation in mitochondria, thus being a specific inhibitor of chloroplast translation (Mulo *et al*. 2003). This enabled the gradual removal of all reaction centre complexes, achieving almost 100% electron transport inhibition, while fully retaining the light-harvesting antenna, LHCII. The effects of inhibition of chloroplast gene translation upon plant growth, cell, chloroplast and photosynthetic membrane structure revealed a remarkable picture of fundamental significance. Firstly, the plants, despite showing some typical signs of senescence, when grown under low light, became well established and sustained their growth for an extended period of time. Secondly, chloroplasts developed supergrana made of bifurcated thylakoid membranes built almost exclusively of light-harvesting complexes. Hence, the profound photoinhibition

Correspondence: A. V. Ruban. e-mail: a.ruban@qmul.ac.uk

did not trigger suppression of the nuclear photosynthetic genes responsible for the formation of the light-harvesting antenna-related proteins. We discuss the structural and functional properties and reasons for existence of the discovered light-harvesting supergrana.

MATERIALS AND METHODS

Plant material and growth conditions

Arabidopsis thaliana cv Columbia was grown in plant growth shelves with a 10 h photoperiod at a light intensity of 90–110 μmol photons $m^{-2}s^{-1}$ and a day/night temperature of 19–28 °C (day); 15 °C (night). Lincomycin (0.2–0.6 g L^{-1}; Sigma Aldrich, Munich, Germany) was added to the irrigation water starting from the rosette stage at 8–9 weeks from sowing. Plants were watered three times per week. F_v/F_m was measured at least two times per week and leaves with desired F_v/F_m were collected for experiments.

Pigment analysis

Total chlorophyll content and chlorophyll *a/b* ratio were estimated from 80% final acetone extract of leaves using Porra method (Porra *et al*. 1989). Intact chloroplasts were prepared as previously described (Crouchman *et al*. 2006; Kiss *et al*. 2008) after 1 h dark adaptation.

Sodium dodecyl sulphate–polyacrylamide gel electrophoresis (SDS-PAGE) and Western blot

The concentration of proteins in total leaf extracts was determined and normalized according to Bradford (1976). The proteins were resolved by SDS-PAGE in a 12% acrylamide gel and transferred onto nitrocellulose membrane. Immunoblotting was performed by incubation with primary antibodies specific for Arabidopsis PsbS protein (Agrisera, Sweden) and CURT1a and b (kind gifts of Prof. Dario Leister). Detection was performed using the ECL Plus Western Blotting Detection System (GE Healthcare Life Sciences, Little Chalfont, UK). Densitometry of the immunosignals was done by NIH ImageJ software and associated plug-ins (http://rsb.info.nih.gov/ij/).

Protein separation

Gel filtration (fast protein liquid chromatography, FPLC) was performed on detergent-solubilized, freshly prepared, stacked thylakoid membranes as described previously (Belgio *et al*. 2012). The thylakoids were suspended to a final chlorophyll concentration of 1.0 mg mL^{-1} and partially solubilized by the addition of n-dodecyl α-D-maltoside to a final concentration of 1% and incubated for 1 min at room temperature. Unsolubilized material was removed by 1 min of centrifugation at 16 000 *g*. The supernatant was then filtered through a 0.45 μm filter and subjected to gel filtration chromatography on an Amersham-Pharmacia Acta purifier system, including a Superdex 200 HR 10/30 column.

Chlorophyll fluorescence

Chlorophyll fluorescence was measured with a Dual-PAM-100 chlorophyll fluorescence photosynthesis analyser (Walz, Effeltrich, Germany) on leaves or chloroplasts (35 μM chlorophyll concentration) using the liquid cell adapter supplied with a cooling system at 18 °C. The chloroplasts reaction medium contained 0.3 M sorbitol, 20 mM tricine, 5 mM $MgCl_2$, 2.5 mM EDTA, pH 7.6. 100 μM of methyl viologen was added as an exogenous electron acceptor. Where mentioned, 200 μM DAD (2,3,5,6-tetramethyl-phenylenediamine in its reduced state) was added to intact chloroplasts to stimulate cyclic electron flow (CEF) around photosystem I (PSI). 6 μM DCMU were used in order to close reaction centres when necessary. Actinic illumination (216 μmol photons m^{-2} s^{-1}) was provided by arrays of 635 nm light-emitting diode (LEDs), the measuring light intensity was 12 μmol photons m^{-2} s^{-1}, maximum fluorescence (F_m) was determined using a 0.8 s saturating light pulse (1000 μmol photons m^{-2} s^{-1}). These light intensities were previously found to give similar excitation pressure (as quantified on the basis of the relative qP levels during actinic light illumination; see Belgio *et al*. 2012) in control and treated leaves. F_v/F_m was calculated as $(F_m - F_o)/F_m$ while qN was calculated as $(F_m - F_m')/F_m$ or non-photochemical quenching (NPQ; $F_m - F_m')/F_m'$. The electron transport rate in function of PAR was obtained using the rapid light curve trig-run program (settings: 2, corresponding to the following light intensities: 0, 45, 66, 90, 125, 190, 285, 420 and 625 μmol $m^{-1}s^{-1}$, 30 s each) and inbuilt fitting (Platt *et al*. 1980) of the Junior-PAM (Walz).

Whole-plant photosystem II (PSII) quantum yield (F_v/F_m) was visualized using a variable chlorophyll fluorescence imaging system (Imaging PAM, Walz) consisting of CCD camera, LED lights and controlling unit connected to a PC running a dedicated software (Imaging Win 2.3, Walz).

Proton gradient determination

ΔpH was determined from the measurement of 9-aminoacridine (9-aa) fluorescence using the Dual-ENADPH and Dual-DNADPH modules for the Dual-PAM-100 chlorophyll fluorescence photosynthesis analyser (Walz). For the titration curve of Fig. 1i, increasing light intensities (70–216 μmol photons m^{-2} s^{-1}) and 200 μM DAD were used to stimulate NPQ. Intact chloroplasts were treated as described above in the presence of 1.4 μM 9-aa. Excitation was provided by 365 nm LEDs and fluorescence emission was detected between 420 and 580 nm.

Freeze-fracture and thin sections transmission electron microscopy

For the freeze-fracture, a dense suspension of thylakoids (prepared as described in Ruban *et al*. 2006) was mounted on flat-topped copper specimen plates, rapidly frozen in slushy liquid nitrogen and fractured at −150 °C in a Polaron E7500 freeze-fracture device (Fisons Scientific Equipment, Loughborough, UK). Replicas were prepared by shadowing with

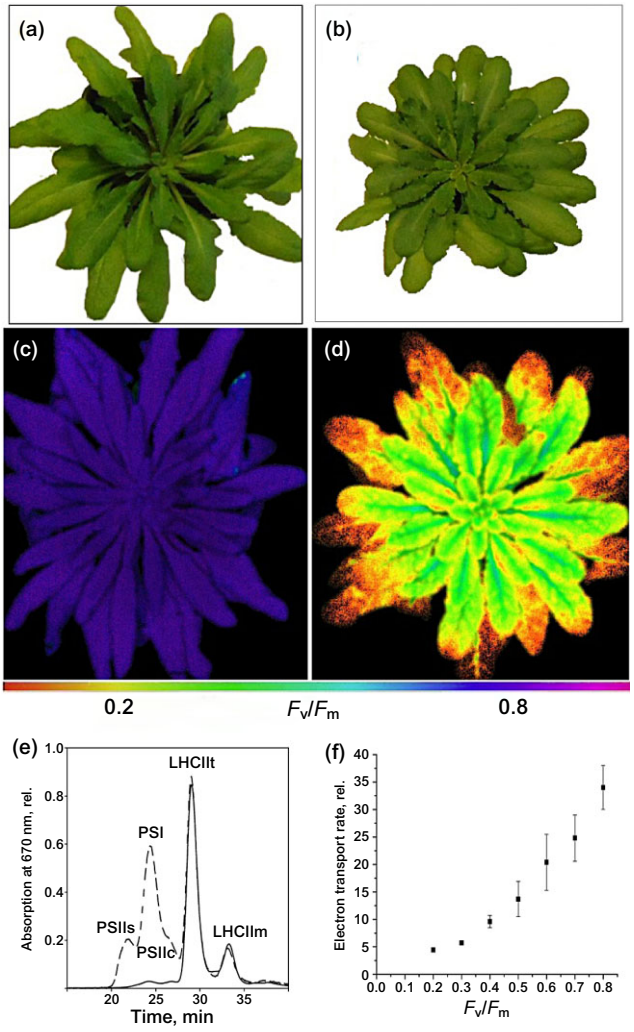

Figure 1. Effect of the absence of the photosynthetic reaction centres on the plant phenotype and the photosynthetic electron transport. Typical aspect of an *Arabidopsis* control plant (a) at the age of 10 weeks compared with a plant of the same age treated for 22 d with the chloroplast gene inhibitor lincomycin (b). Chlorophyll fluorescence imaging of F_v/F_m of control (c) and treated (d) plants, images normalized to the false-colour bar provided. The pixel value display is based on a false-colour scale ranging from black (0.00 to 0.040) via red, yellow, green, blue to purple (ending at 1.00). (e) Chromatogram of gel filtration runs of solubilized stacked thylakoids from treated ($F_v/F_m = 0.03$, solid line) and untreated plants (dashed line). Spectra were normalized to the maximum of absorption at 670 nm. (f) Plot of electron transport rate as a function of F_v/F_m. Each data point was determined using an inbuilt trig-run program for rapid light curves and relative fitting function from Junior-PAM (light intensities were 0, 45, 66, 90, 125, 190, 285, 420 and 625 μmol $m^{-1}s^{-1}$; for more details, see Methods).

platinum at an angle of 45° and carbon at an angle of 90°. They were cleaned in a 1:2 dilution of household bleach (3–6% sodium hypochlorite) in distilled water. Freeze-fracture replicas were examined with a Jeol 1230 transmission electron microscope (JEOL USA, Inc., Peabody, MA, USA) at a range of magnifications. The coordinates and dimensions of particles on the exoplasmic fracture faces (EFs) and periplasmic fracture faces (PFs) of freeze-fracture electron microscopy images were identified with particle picker routines using ImagePro Plus software (Media Cybernetics, Rockville, MD, USA). Nearest-neighbour distances and particle clustering were calculated from the coordinates of each particle using a bespoke program (available on request). Nearest neighbour distance analysis of freeze-fracture EM images allows to measure the distances with 0.72 nm accuracy, which is the spatial resolution (single pixel size in XY direction) of our electron micrographs. If there is a change in the distance between two particles, the program would only detect the difference at the level of at least one single pixel size). For thin sections, small pieces of leaves were fixed in 3% (v/v) glutaraldehyde, 1% (w/v) paraformaldehyde and 0.5% (w/v) tannic acid in 0.05 M Na-phosphate buffer, pH 7.0 for 2 h at room temperature. After rinsing in 0.1 M Na-phosphate buffer overnight, the samples were post-fixed with 2% (w/v) osmium tetroxide in 0.1 M Na-phosphate buffer, pH 7.0 for 2 h at room temperature, dehydrated through a graded acetone series and embedded in Araldite CY212 via acetone. Ultrathin sections were sequentially stained with saturated aqueous uranyl acetate and Reynold's lead citrate. Number of thylakoids per granum, number of plastoglobuli and the volume occupied by starch were calculated from these ultrathin section images using ImagePro Software (Media Cybernetics). Total leaf biomass was calculated with the same software from individual pictures taken at different stages of development.

Confocal microscopy

Leaf discs were soaked in 0.9 M aqueous sucrose solution for 2 h in the dark and mounted on glass slides. Documentation was performed with a Leica SP5-TCS confocal laser scanning microscope (Leika Microsystems Ltd., Milton Keynes, UK) using a 63× oil immersion lens. The confocal image stacks were analysed with the 3D-reconstruction software IMARIS (Bitplane AG, Zurich, Switzerland).

RESULTS

Plant and leaf structure and photosynthetic function

Figure 1a,b displays *Arabidopsis* plants at the rosette stage, untreated (a) and treated (b) with lincomycin for 22 d. The plant continued to grow during the treatment, but developed profound signs of photoinhibition that could only be detected by the pulse amplitude modulated (PAM) fluorescence. The false-colour images of the PSII quantum efficiency (yield, F_v/F_m) are shown in Fig. 1c,d. The treatment caused a reduction of F_v/F_m from 0.8 to eventually zero fairly homogeneously throughout the leaf age and area in all leaves. Despite the strong photoinhibition, growth rates were not affected, as the total leaf biomass was similar to the control (150 $cm^2 \pm 25$ at the 22nd day of treatment), and no significant biomass difference was observed throughout the whole treatment (data not shown). For leaves with $F_v/F_m = 0.2$ the

total chlorophyll content was decreased by about 35% (normalized on total leaf wet weight), and the average chlorophyll *a/b* ratio dropped from 3.4 to 2.3, indicative of the profound change in the composition of pigment-protein complexes. For leaves with $F_v/F_m = 0.03$ the almost complete elimination of both PSII and PSI complexes (devoid of chlorophyll *b*) with respect to the amounts of LHCII complexes was observed. Indeed, Fig. 1e shows FPLC gel filtration profiles of solubilized thylakoids from control (dashed line) and treated (solid line) plants possessing $F_v/F_m = 0.03$. The latter showed total disappearance of PSII supercomplexes band at around 22 min of elution, although small traces of PSII monomeric cores were still present (26 min elution peak). In addition, the amount of PSI was also reduced by approximately 10 times in comparison to the control. On the contrary, amounts of trimeric (29 min elution peak) and monomeric (33 min elution peak) LHCII complexes appeared to be unaffected by the treatment.

Strong reduction in the PSII yield during the course of the treatment was followed by an even steeper decrease in the electron transport rate consistent with the fact that PSI concentration was also dramatically reduced in the treated plants (Fig. 1f). This was not surprising considering that many components of the electron transport chain, like the Rieske iron sulphur protein, the ferredoxin NADP oxido-reductase and also the oxygen evolving complex, are chloroplast encoded, therefore expected to be undermined by the treatment.

Confocal fluorescence microscopy

In order to gain information concerning the chloroplast and photosynthetic membrane structure of lincomycin-treated plants, we undertook microscopic studies. Firstly, the chlorophyll fluorescence confocal microscopy of chloroplasts in intact leaves was applied. The study revealed remarkable alterations in the structure of chloroplasts of the treated plants (compare Fig. 2a,b). While chloroplasts of control plants possessed literally hundreds of fine round-shaped grana (visible as red little grains of <500 nm diameter), the chloroplasts of treated plants contained much fewer but larger round and often oval structures reaching 2 μm in size. The chloroplasts themselves of the treated plants were slightly smaller in size and often of spherical shape.

Electron microscopy reveals the structure of the supergrana

The transmission electron microscopy of these intriguing structures using ultrathin sections of negatively stained samples showed that the big grains are extremely large grana often made of several hundreds of thylakoids (Fig. 2c–f). The size of a single thylakoid membrane of these giant formations was often much bigger and the membrane area of one such supergrana was about 100 times larger than that of the grana of control chloroplasts, extending to a few millions of square nanometres (compare Fig. 3a,b). Bar charts in Fig. 3c,d show the percentage distribution of thylakoids in control and treated samples, with the average total membrane area in a

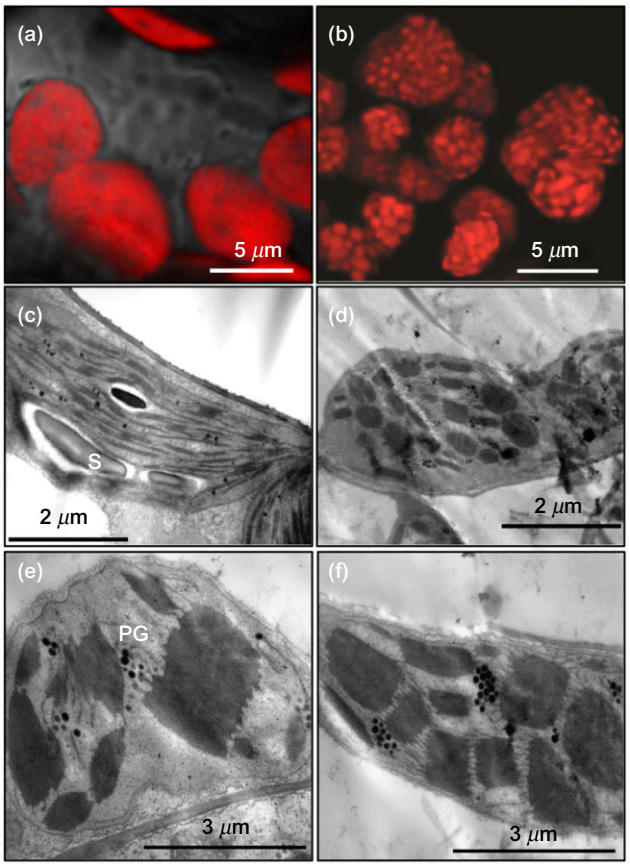

Figure 2. Fluorescence confocal and transmission electron microscopy of chloroplasts from control and treated intact leaves. (a, b) Confocal fluorescence images of chloroplasts from treated (b) and control (a) plants displaying individual grana as intense spherical or oval grains of variable sizes. Ultrathin sections of control (c) and treated (d, e, f) leaves showing chloroplast ultrastructure (grana) at different magnifications. PG, plastoglobuli; S, starch.

single supergrana reaching 500 μm^2. As a consequence, stroma lamellae were relatively diminished, confirming our previous finding of reduced amounts of PSI supercomplex in the treated membranes. This indicates that one chloroplast of treated plants that contains 10 supergrana can possess the membrane area of approx. 70×70 μm.

Another interesting feature of chloroplasts from treated plants is that they contain very little starch. While the control chloroplasts possessed up to 10% of starch of the total volume of chloroplasts, the treated plants' chloroplasts contained less than 1% (Fig. 3e). In addition, chloroplasts of treated plants contain many plastoglobuli – vesicles that carry lipids, enzymes, quinones and antioxidants (Nacir & Bréhélin 2013). They are often positioned in the regions of unstacked thylakoids in groups of about a dozen vesicles (Figs 2c–f & 3a,b) and are at least three times more abundant in the treated sample (Fig. 3e). The appearance of plastoglobuli is thought to be associated with the onset of senescence and abiotic stress (Nacir & Bréhélin 2013), as in our case – a profound lincomycin-stimulated photoinhibition. It

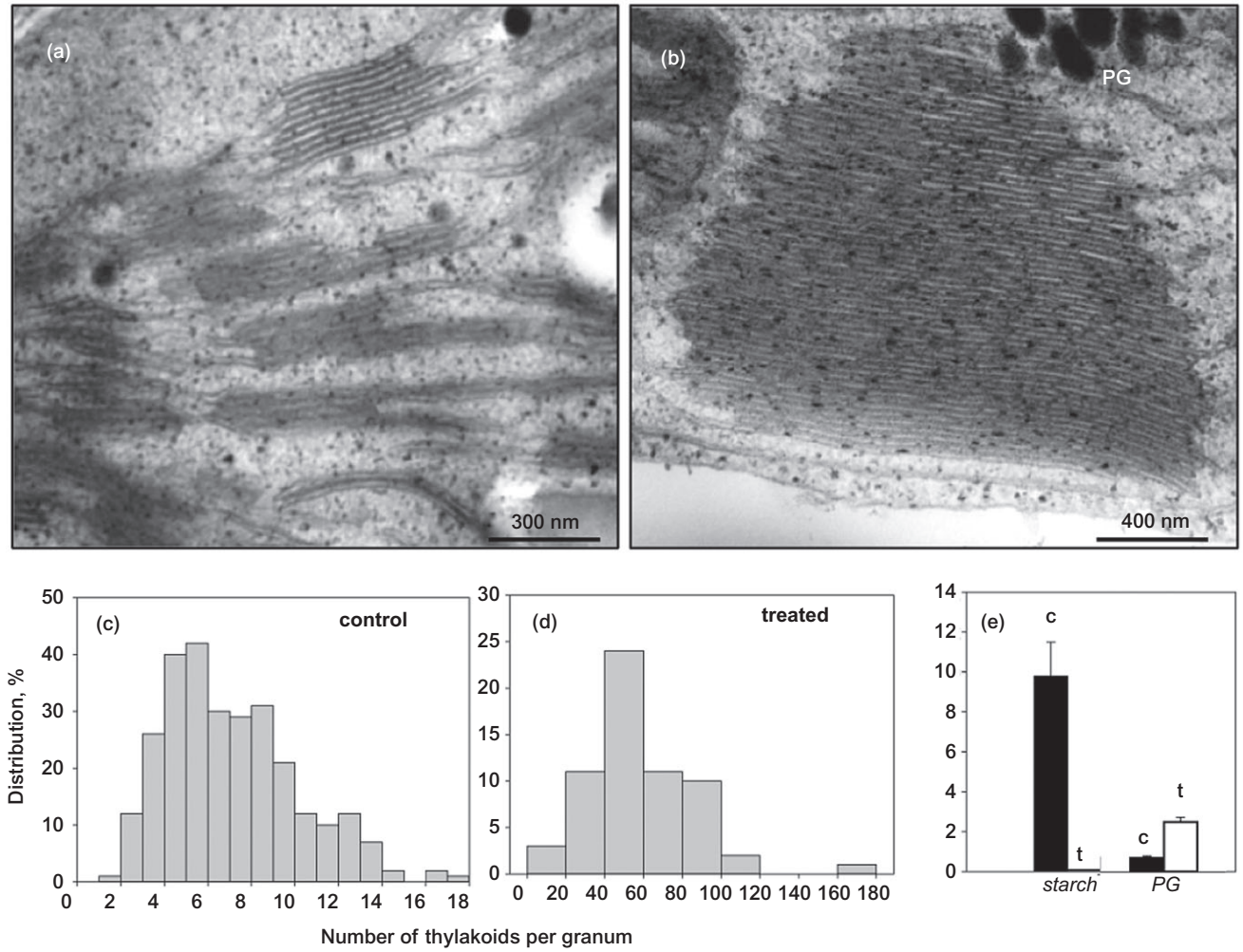

Figure 3. Analysis of ultrathin transmission electron microscopy sections. Control (a) and treated (b) leaves displaying individual thylakoids of grana at high magnification. (c, d) Bar charts showing the percentage distribution of the number of thylakoids of control and treated samples estimated from thin sections. (e) Bar chart showing the percentage distribution of starch (left) and plastoglobuli (PG, right) per volume of control (c) and treated (t) chloroplasts quantified from the ultrathin sections analysed. Error bars represent standard errors for 10–12 chloroplasts analysed.

is plausible that the enzymatic systems of these vesicles are being prepared for demolition of the thylakoid membranes (starting from the unstacked membranes) in case the photoinhibited state continues, and in order to use the membrane components as a source of metabolic energy/material. Apart from plastoglobuli, treated plants also displayed other senescence-like symptoms, such as osmiophilic deposits of lipids and whorls of membranes (Supporting Information Fig. S1), which are residues of an authophagic process from the vacuole engulfing organelles (Nooden 1988). These preliminary signs, however, did not lead to the next stage of senescence, usually characterized by chlorophyll bleaching, disappearance of thylakoid membranes and, eventually, leaf necrosis. Such manifestations were absent, the treated plants being capable of sustaining their peculiar, incomplete senescence, for the whole duration of the treatment (>12 weeks).

The existence of supergrana prompted us to screen a variety of replicas of freeze-fractured projections of chloroplasts from lincomycin-treated plants. The peculiar structural characteristics of the treated membranes allowed us to obtain for the first time fractures along the side of the grana stacks. Figure 4 shows these projections. The occurrence of these side fractures can be explained by the large size of the supergrana that enhanced the frequency of fractures that take place along the surfaces of grana margins with the water phase of the chloroplast stroma (Fig. 4a,b). These fractures explicitly revealed the existence of multiple fusions or branching (bifurcations) of individual membranes (Fig. 4c–f). These features have been predicted in the structural work of Reich's group using the computer-reconstituted cryo-electron tomography imaging analysis (Shimoni *et al*. 2005; Nevo *et al*. 2012). This work is being opposed by several different views upon the grana organization, most noticeably by Garab's group (Mustárdy & Garab 2003) and Arvidsson & Sundby (1999; for review, see Nevo *et al*. 2012). While Mustárdy and Garab suggest the existence of helical

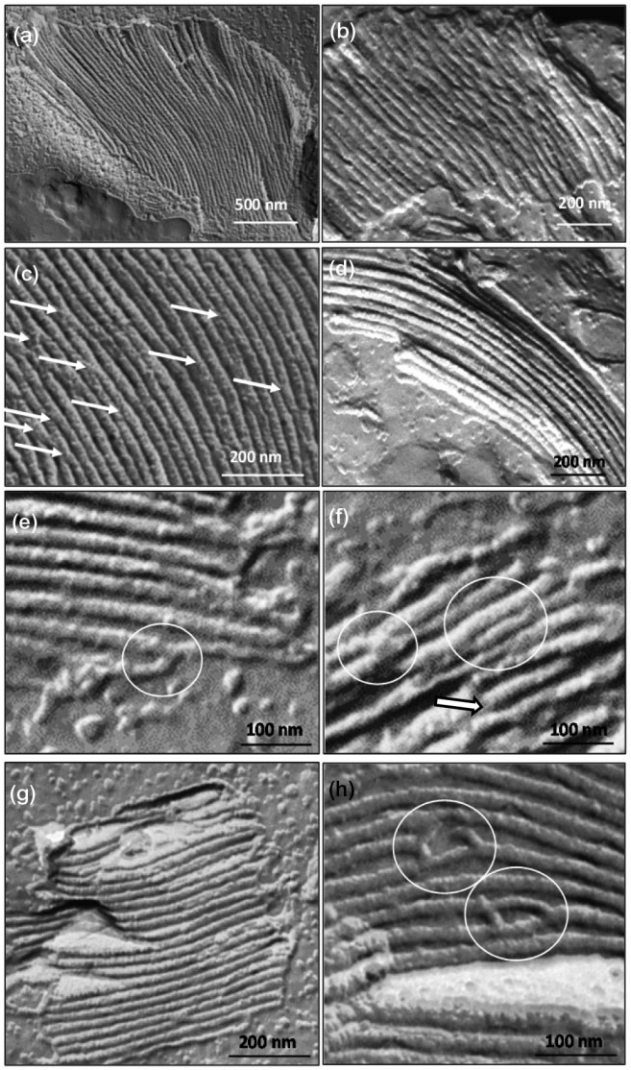

Figure 4. Transverse fractures of the grana stacks. (a–h) Aspect of freeze-fractured treated membranes ($F_v/F_m = 0.2$) where the fracture occurred along the transversal side of the membrane, at three different magnifications. In c, the arrow points at multiple fusions or branching of individual membranes. Multiple bridges between thylakoids are circled in e, f and h.

organization of the grana, Arvidsson and Sundby proposed folding of a single membrane into the granal structure. Our freeze-fracture imaging of side-fractured grana revealed the existence of multiple bridges between thylakoids of grana as a result of membrane bifurcations. Figure 4f is particularly interesting. It displays one such bridge (on the left) and one closely positioned bridge (near the centre) that form a 'bubble' of stromal space. The bottom central part of the figure shows the existence of triple branching (see arrow in Fig. 4f). Figure 4g depicts almost a three-dimensional replica of the supergranal fragment that indicates the sheer complexity of the structure with thylakoids of variable size, shape and connectivity. Figure 4h shows an enlarged side view of almost separate thylakoids in the grana, with the only elements that hold it together being not direct van der Waals or ionic interactions, but bifurcated or fused parts of thylakoid membranes (encircled). Hence, the grana seem to be organized as a sponge-like three-dimensional structure.

PSII particle densities

In order to study the changes in populations of PSII and LHCII complexes and their densities in the grana membranes, we employed freeze-fracture electron microscopy. The freeze-fracture technique splits hydrophobic core of the membrane bilayer into the exoplasmic and protoplasmic leaflets, allowing information on the organization and dimensions of the proteins therein to be determined by image analysis. Four distinct fracture faces are observed in freeze-fracture EM images (reviewed in Staehelin 2003). The EF of the stacked membranes is dominated by PSII particles of ~16 to 18 nm correspondent to core dimer plus 2–3 monomers (Staehelin 1976; Armond *et al*. 1977). The complementary protoplasmic fracture face of the stacked membranes (PFs) contains ~8-nm LHCII particles, corresponding to LHCII trimers (Miller *et al*. 1976; Simpson 1979). The protoplasmic fracture face of the unstacked membranes is distinguished on the basis of its slightly larger asymmetric ~10 nm PSI particles (Simpson 1982). Finally, the complementary EF of the unstacked membranes is largely smooth and marked by generally more widely spaced ~10 to 16 nm PSII particles (Staehelin 1976; Armond *et al*. 1977; Johnson *et al*. 2011). Figure 5a,b shows the density of RCII complexes in the membranes of control plants, while Fig. 5c,d shows that the density of PSII in treated plants that possess F_v/F_m ratio of 0.4 are much lower. Continuing lincomycin treatment lead to the further reduction in number of RCII complexes and decrease in the yield to about 0.2 while LHCII particle density appeared to remain unchanged in the PFs fracture faces (Fig. 5e).

Statistical analysis presented on Fig. 6 confirmed these observations and revealed that the density of RCII complexes was strongly decreased in the treated plants from 10–11 PSII particles to ~1 within 50 nm radius, in agreement with 10% remaining RCs, as previously quantified by SDS-page (see Belgio *et al*. 2012). Within the resolution of the method (~1 nm), the size of the PSII particles was not significantly different from control. Since these particles represent PSII core dimer plus 2–3 minor antenna proteins (~220 nm^2; Armond *et al*. 1977; Boekema *et al*. 1995), this observation confirmed that the treatment did not induce, unlike trimers, significant increase in the concentration of minor complexes. The density of LHCII particles was comparable to the control, with a bulk (70–80%) of 7–8 LHCIIs localized within 25 nm radius. The striking similarity, considering the huge decrease in PSII complexes, points at the robustness of LHCII organization in the photosynthetic membrane. It is interesting to notice in this context that an increase in LHCII by a similar extent, ~30% was quantified for the treated sample via Western blotting confirmed by FPLC (Belgio *et al*. 2012). This increase is due to an unknown feedback mechanism from the chloroplast (see Discussion). It is therefore reasonable to suggest that the slightly higher density found in

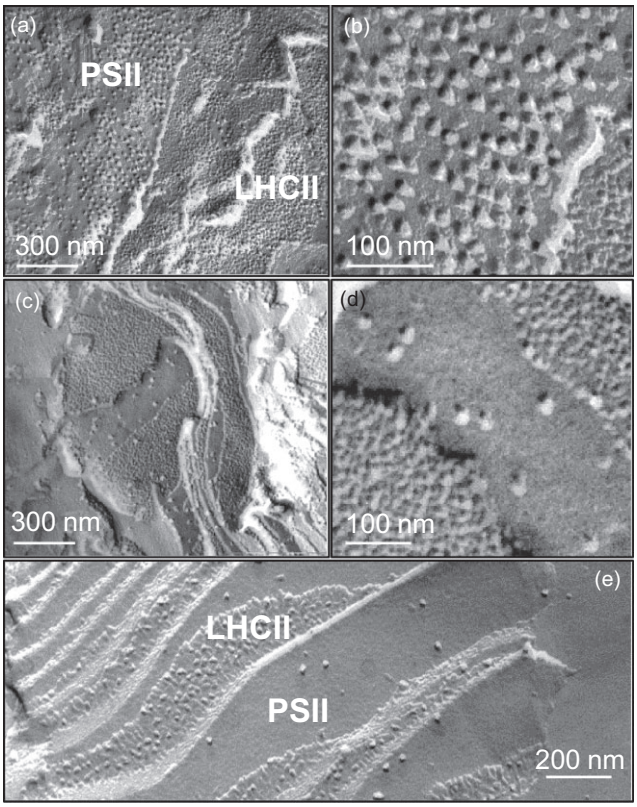

Figure 5. Freeze-fracture electron microscopy of photosystem II complexes in grana membranes. Electron micrographs showing the thylakoid membrane structure of control (a, b) and treated (c, d and e) plants. PSII and LHCII complexes are located on the exoplasmic and periplasmic fracture faces, respectively. F_v/F_m was 0.8 (a, b), 0.4 (c, d) and 0.2 (e).

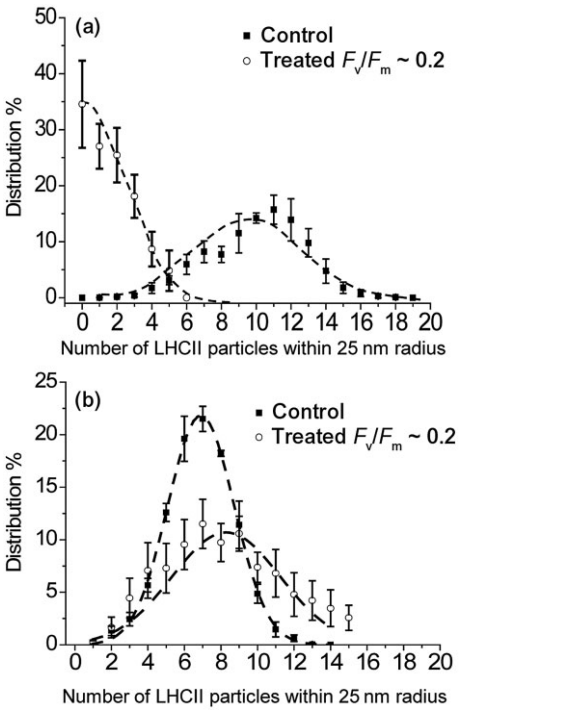

Figure 6. Analysis of the particle densities on the freeze-fracture electron microscopy images of grana membranes. (a) Graphs showing the percentage distribution of PSII clustering (number of neighbouring PSII particles within a 50 nm radius of a given PSII particle) of control (squares) and treated (circles) thylakoid membranes. F_v/F_m of the treated sample was 0.2. (b) Graphs showing the percentage distribution of LHCII clustering (number of neighbouring LHCII particles within a 25 nm radius of a given LHCII particle) of control (squares) and treated (circles) thylakoid membranes. F_v/F_m of treated sample was 0.2. In all cases, leaves were dark-adapted for 1 h before thylakoid isolation. Each data point represents a mean value (SE) for all EFs and PFs fracture faces analysed (n = 4–19). The lines are fitted Gaussian curves (Originlab 7.5).

the treated membranes corresponds to the relative increase in LHCII. Indeed, the bulk population of LHCII has been demonstrated to be uncoupled or very poorly coupled to the few RCs remaining after lincomycin treatment (Belgio *et al*. 2012). Nevertheless, the fluorescence state was found to be similar to that of the control at Fm (2 ns), leading to the conclusion that the state of LHCII in the photosynthetic membrane is different from the 4 ns unquenched one, typical of detergent-isolated LHCII. This 'intermediate' fluorescence membrane state has therefore been called 'pre-aggregated', to indicate its readiness to become highly quenched and aggregated under high light (Belgio *et al*. 2012; Petrou *et al*. 2014). It is interesting to notice that, likewise the lincomycin-treated membranes, ~80% of LHCII was found to be poorly coupled to PSII in *Chlamydomonas*. Similarly to our findings, the uncoupled antenna there displayed high quenching under light, a mechanism considered to be protective from photodamage (Iwai *et al*. 2010; Ünlü *et al*. 2014).

PAM fluorescence analysis

One remarkable feature of the treated plants was that, despite the decline in the PSII yield and electron transport rate, they exhibited increased levels of NPQ – a major molecular mechanism that protects the photosynthetic centres against photoinhibition (Ruban *et al*. 2012). The increase in NPQ had previously been quantified to be more than 50% for plants with F_v/F_m of ~0.2 (Belgio *et al*. 2012). In the present study, we determined for the first time the relationship between F_v/F_m and NPQ amplitude in live plants (Fig. 7, bottom) using the same routine as in the preceding paper (Supporting Information Fig. S2). Briefly, control and treated leaves were exposed to 2 × 5 min actinic light illumination, each followed by 5 min dark recovery. At the end of the second illumination cycle, NPQ was measured and plotted against F_v/F_m. The relationship followed a clear bell-shaped trend centred about F_v/F_m~0.35 and corresponding to a level of NPQ (K_d) of approximately 2.3. In plants with F_v/F_m of ~0.05, the level of NPQ decreased to 0.5, about half of the control level. The lowest NPQ (~0.2) was found in plants with F_v/F_m~0 (marked with a triangle in Fig. 7g, bottom). The observation that plants with F_v/F_m of 0.35 had the maximum NPQ level suggested that the remaining PSII complexes (~10% of control, see Fig. 6a and also Belgio *et al*. 2012) and

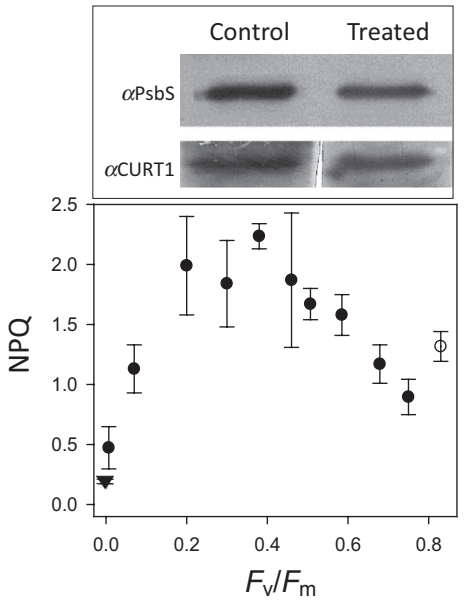

Figure 7. Dependency of NPQ upon the concentration of PSII reaction centre complexes. NPQ ($K_d = (F_m - F_m')/F_m'$) was plotted as a function of F_v/F_m as determined by Dual-PAM-100 (Walz) for control ($F_v/F_m = 0.8$) and leaves with different extent of treatment ($F_v/F_m = 0.007$–0.75, circles; $F_v/F_m = 0$, triangle) under 216 μmol photons m^{-2} s^{-1}. Top panel is a Western blot analysis of the amount of PsbS and CURT1 proteins in the membranes of control and lincomycin-treated plants.

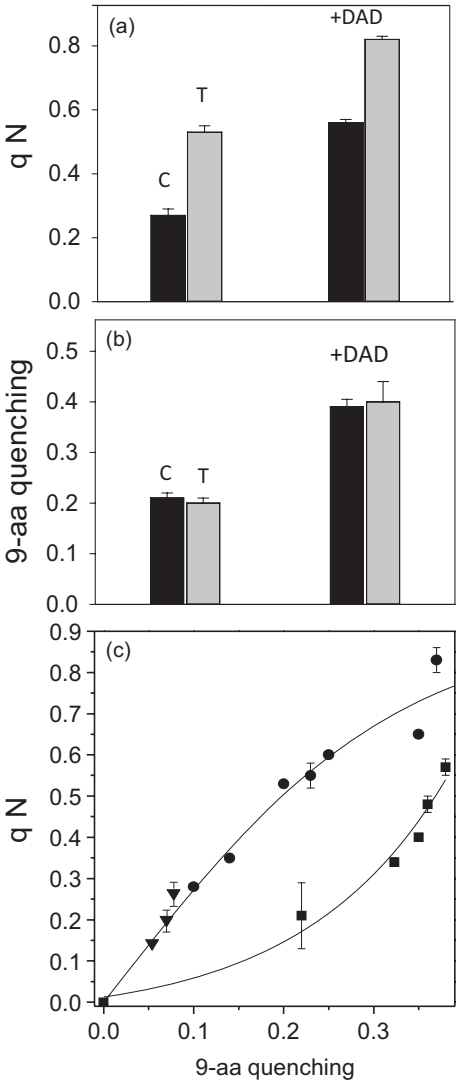

Figure 8. Relationship between NPQ and proton gradient in the isolated chloroplasts from control and lincomycin-treated plants. (a) Top: bar chart showing NPQ (expressed as qN: $(F_m - F_m')/F_m'$) of control (C, black) and treated (T, grey) chloroplasts without (left) and with (right) 200 μM DAD. F_v/F_m of treated leaves was 0.4. (b) Comparison of 9-aa quenching in the same chloroplast samples as used for then data displayed in panel a in the absence (left) and presence (right) of 200 μM DAD. (c) Titration curve of NPQ (qN = $(F_m - F_m')/F_m$) in function of 9-aa quenching for control (squares) and treated ($F_v/F_m = 0.4$, circles; $F_v/F_m = 0$, triangles). The function used for the fitting was a three Hill Sigmoidal from the Sigmaplot software. F_v/F_m of treated leaves was 0.4. All error bars represent standard errors calculated from more than three independent samples.

electron transport rate (less than 30% of the control, see Fig. 1f) were still capable of maintaining a sustained proton gradient (ΔpH) across the photosynthetic membrane, an indispensable element of NPQ formation. In order to test this possibility, quenching of 9-aminoacridine dye – an indicator of ΔpH – was measured in chloroplasts from treated leaves (F_v/F_m~0.35). They displayed a 50% increase in an NPQ parameter qN, confirming the results obtained on leaves (Fig. 8a) although the levels of the proton gradient were very similar to the control (Fig. 8b). Interestingly, the use of the proton shuttle diaminodurene (DAD) induced similar ΔpH in both types of plant material, treated and control, despite a 30% greater enhancement in NPQ in the treated sample. This fact suggests that NPQ in the treated plants is simply more sensitive to protons, possessing a somewhat higher pK value (Petrou *et al*. 2014). The treated sample, in fact, displayed a higher degree of cooperativity in the titration curve of qN against 9-aa quenching (Fig. 8c). It is important to mention in this context that the level of PsbS protein was not increased in the treated plants, in agreement with a previous report (Belgio *et al*. 2012; Fig. 7, top). Similarly, the HPLC analysis confirmed that there was no difference in the zeaxanthin content of the two types of plants (data not shown, see also Belgio *et al*. 2012). Since the electron transport chain components responsible for increased CEF are chloroplast encoded, they are unlikely to be enhanced in the treated plants (Livingston *et al*. 2010). An alternative explanation for the similar ΔpH in the treated plants is that the reduction of three chloroplast-encoded subunits of ATPase (α, β and ε, see, e.g. Woessner *et al*. 1987) could contribute to the sustaining still high levels of ΔpH in conditions of reduced electron transport and PSI. Moreover, it has been previously shown that ΔpH is proportional to a vesicle lumen capacity (Harrigan *et al*. 1992). Since the treated plants displayed increased number of chloroplasts with reduced dimensions compared with control (see also Fig. 2), one possibility is also that the relative chloroplast-lumen volume is reduced. In this

context, a few protons pumped across the thylakoid membrane would be sufficient to yield a sustained delta-pH (which in turn could not be dissipated by low content of ATP synthase). Interestingly, plants with $F_v/F_m = 0$ still possessed NPQ, albeit at low levels, and a proton gradient most likely generated here by a small remainder of PSI engaged in cyclic electron transport (see Fig. 1e).

Altogether, these observations point out that the structural environment of the LHCII antenna in the treated plants is likely to be somewhat different from that of the control plants making their antenna more sensitive to lumen pH. In this respect, it is important to point out that the data in Fig. 6b show that a minor population of LHCII particles (~25%) undergoes stronger clustering in comparison to that of the untreated plants. Since recent studies suggested that protein aggregation by promoting the hydrophobicity of the environment of proton-receiving amino acids of LHCII accelerates the dynamic switch of LHCII into the photoprotective state (Ruban 2012; Ruban *et al*. 2012; Petrou *et al*. 2014), the enhanced clustering of LHCII in the treated membranes may provide an explanation for the observed increase in the pH sensitivity of NPQ in the treated plants (see Fig. 8c). Indeed, the ΔpH titration curve presented on Fig. 8c of NPQ in chloroplasts isolated from treated plants is strongly shifted towards lower levels of ΔpH. Since the levels of PsbS or zeaxanthin were similar to the control, the only explanation for this shift could come from the possibility that enhanced LHCII clustering/aggregation could be due to removal of RCII core complexes that makes structural spaces LHCII to interact with itself at the absence of the PSII supercomplex structure. The latter is likely to play a role of structural vector restricting LHCII rearrangement towards the aggregated state and/or providing an environment that diminishes formation of hydrophobic domains within the complex.

DISCUSSION

The fine structure of thylakoids in the supergrana

We have discovered an outstanding consequence of the decrease in the concentration of RCII complexes – the formation of supergranal structures built largely of LHCII trimers and monomers. These structures possess a very large membrane surface and accumulate millions of LHCII trimers – an attractive model of the three-dimensional natural light-harvesting unit. Indeed, recent studies showed that two-dimensional aggregated LHCII immobilized upon TiO_2 possesses enhanced ability to sensitize the reductive (Lee *et al*. 2014) or photovoltaic (Yang *et al*. 2014) properties of the semiconductor that was explained by the enhancement of chlorophyll–chlorophyll charge transfer states (Miloslavina *et al*. 2008; Holzwarth *et al*. 2009) in densely clustered, aggregated LHCII complexes. Hence, the three-dimensional matrix of the complex could be an important step forward towards radical enhancement of productivity of the hybrid assemblies.

The new plant system offers several advantages compared with traditional mutants lacking PSII (see, e.g. Bennoun *et al*. 1986; Vallon *et al*. 1986; Simpson *et al*. 1989). By adjusting the concentration of the antibiotic and/or duration of the treatment, PSII concentration can be gradually reduced. This allows the monitoring of the physiological consequences of a progressive reduction of PSII. Also of advantage is the unexpected finding of a similar leaf biomass to the control, which is especially appealing for photovoltaic applications (see above). Moreover, the treatment here reported can in the future be applied to other plant species besides mutants lacking PsbS, zeaxanthin or minor antennas, for example, to see the combined effect of treatment and mutations. Finally, the consequences of the treatment on the general plant physiology can be of potential interest for senescence studies and feedback regulation (see below). The supergrana revealed frequent membrane bifurcations that are likely to be the major structural factor that stabilizes stacking. Giant grana have been previously observed in rare plants grown under very shaded environment (Jia *et al*. 2012). Indeed, abaxial cell layers of *Trapa natans* leaves floating on the water surface displayed giant grana (Bassi 1986; Nedukha 2012). Interestingly, also in this case, the abnormal grana structure was accompanied by a decrease of starch grains, decrease of chl *a/b* ratio and total chlorophyll, similarly to the lincomycin-treated plants. Low light environment was known to induce better grana stacking, resulting in increased number of thylakoids per granum. This was interpreted as a result of the enhanced concentration of LHCII complexes (Anderson *et al*. 2008). The underlying molecular mechanism, however, is still debated. It is well known that surface charges affect thylakoid structure and function (Barber 1982). However, neutralization of negative charges on the surface membrane by addition of Mg^{2+} is effective only in the presence of LHCII, since mutants lacking LHCII showed poor stacking (Allen *et al*. 1988). Indeed, the popular idea of LHCII as promoter of stacking is connected to the physical segregation of granal PSII from PSI, which, in higher plants, provides the advantage of limiting excitation energy 'spillover' (Trissl & Wilhelm 1993; Mullineaux 2005). Earlier work on wheat treated with chloramphenicol demonstrated enhanced accumulation of LHCII complexes that correlated with formation of very long granal stacks; however, containing almost the same number of thylakoids as the control (Duysen *et al*. 1985), again clearly indicative that LHCII antenna proteins are one of the key contributors to formation of large granal stacks. Recently, plants overexpressing CURT1, a protein proposed to be crucial in defining thylakoid curvature, possessed 1.63 times more thylakoids in a single grana than control (Armbruster *et al*. 2013). However, the concentration of this protein was not increased in the treated plants (see Fig. 7), thus excluding its active role in formation of supergrana. Increase in the grana size has been also observed in *Arabidopsis* double mutant *adg1-1/tpt-1* deficient in starch biosynthesis (Häusler *et al*. 2008). These plants, unlike lincomycin-treated ones used in our study, revealed an enhanced reduction of the electron transport chain and reduction in the growth rate. The area of

enlarged grana was however only two times larger than that of the control and, as in our system, there was an increase in the number of plastoglobuli. Although the authors also observed reduction in PSII yield, it was not known whether LHCII/PSII ratio was enhanced in the *adg1-1/tpt-1* mutant. Interestingly, those plants revealed reduced levels of NPQ/qE unlike the ones used in our study (Fig. 8).

Despite the evidence for LHCII being important for grana stacking, the idea of LHCII as the only determinant seems an oversimplification. Early reports (Bassi *et al*. 1985) showed that the chl *b*-less barley mutant chlorina-f2 exhibits grana stacking at levels similar or higher than control. Recently, however, the *ch1-3* mutants were instead found to be not well stacked, an effect attributed to lower van der Waals forces, diminished electrostatic attraction between opposite membrane layers and instability of PSII supercomplex in the absence of LHCII (Kim *et al*. 2009). In the light of our data, we suggest that the exceptionally large increase in grana size of the lincomycin-treated plants be due, rather than to the slight increase of LHCII by itself, to the decrease of RCII. Indeed, *viridis*^{115}, the barley mutant completely lacking PSII complexes (Simpson *et al*. 1989), displayed five times larger grana than control. Previous studies on NPQ already pointed at PSII as an organizer of the lateral dynamics/fluidity of LHCII in the thylakoidal membrane (Johnson *et al*. 2011; Belgio *et al*. 2012). In this scenario, RCII would appear to be a complex that actually prevents the large scale stacking – an 'anti-stacking' complex, which can be counterbalanced by LHCII 'stacking-promoter'. This model would fit well the evidence of normal stacking in the absence of both PSII and LHCII in the double mutant *clo-f2*^{2800}-*viridis*^{115} (Simpson *et al*. 1989). PSII complex may perform its anti-stacking function by limiting the frequency of the observed bifurcations (Fig. 4) that weaken the grana-stabilizing forces. Therefore, it seems that LHCII-containing membranes acquired a property for branching that aids the ease with which grana structures are formed.

NPQ in the absence of PSII

This work revealed a remarkable functional response of the thylakoid system to the gradual removal of photosystem complexes. Relatively established plants sustained their viability and growth for a prolonged length of time (>12 weeks), even in conditions of profound down-regulation of a number of RCII complexes. This fact suggests that the effect of photoinhibition on the plant well-being may not be as obvious as previously thought. If plants at the start of the treatment are relatively well established and contain significant amounts of stored glucose in the form of starch, they can cope well with photoinhibition at the cost of few sustained signs of senescence and increased NPQ. Hence, the mentioned controversy about the effect of photoinhibition on the crop yield and plant well-being in general may well originate from the increasingly vague connection between the efficiency of the electron transport and carbon assimilation upon the maturation of the plant organism. Several reports have shown LHCII accumulation in response to stress (Guiamet *et al*. 2002; Caffarri *et al*. 2005; Ware *et al*. 2015). In lincomycin-treated plants, a large amount of these extra LHCIIs is uncoupled from RCs (Belgio *et al*. 2012). The poor energetic connectivity thus makes photochemical quenching ineffective, as indicated by typically high Fo fluorescence levels. Despite this, under high light, the 'loosen' LHCII complexes still become highly quenched, resulting in significantly higher NPQ, once more pointing at the profound difference between photochemical and non-photochemical, antenna-based, quenching. It is interesting to notice that quenching of a pool of detached LHCIIs has been recently reported to occur in *Chlamydomons*. In this organism during state transitions, LHCII apparently detaches from PSII without connecting to PSI (Drop *et al*. 2014; Ünlü *et al*. 2014). Similarly to what happens in the lincomycin-treated membranes, quenching of detached LHCII seems to be a necessary physiological response to avoid photodamage also in the algae. However, it must be noted that control, not stressed plants, normally display good functional connection between LHCIIs and RCs. This connection has recently been shown to be even increased under illumination (Belgio *et al*. 2012), thus pointing at a much higher complexity of physiological responses that higher plants can adopt in response to high light compared with *Chlamydomons*. The enhanced NPQ thus can be interpreted as functional for the plant that tries to maximize the photoprotective capacity in order to prevent the detrimental effect of photoinhibition, as well as protect the antenna itself at the absence of the energy sinks – reaction centres. It seems that the ratio between RCII and LHCII complexes and their connectivity in the higher plant photosynthetic membrane is inherently and fundamentally crucial in defining the extent of photoprotection that is required for plant survival.

The consequence of the lack of a retrograde signalling pathway

Our results here confirm the previous finding that lincomycin treatment not only affected RC translation, but, via a retrograde feedback mechanism, induced the increase of the nuclear-encoded LHCII protein. The redox state of the electron transport chain has indeed a crucial role in the retrograde signalling that controls nuclear gene expression of LHCII antenna proteins (Escoubas *et al*. 1995; Petracek *et al*. 1997; Pfannschmidt 2003; Chen *et al*. 2004; Nott *et al*. 2006; Eberhard *et al*. 2008). It has been previously shown that low temperature (13 °C)/high light (1000 μmol photons m^{-2} s^{-1}) growing conditions led to a decrease in concentration of RC, CP29 and CP26 complexes in *Zea mays* plants as opposed to enhanced LHCII accumulation and 40% higher NPQ (Caffarri *et al*. 2005). Retention of LHCII complexes was similarly found in the Arabidopsis mutant cytG, where senescence-induced degradation of all photosynthetic proteins but LHCII, demonstrating that regulation of LHCII follows a different, independent pathway from other antennas (Guiamet *et al*. 2002). Since our plants grew at very low light intensity, it seems reasonable to think that the gradual disappearance of RCIIs was not followed by overreduction

of the electron transport chain or formation of reactive oxygen species that could generate retrograde signals aimed to inhibit Lhcb genes. At these conditions, the nucleus seems to be completely 'unaware' of the huge losses in reaction centres simply because they were not associated with the highly reduced state of the plastoquinone pool and photoinhibitory damage resulting in formation of reactive oxygen species but rather emerged as a result of the consequences of their 'wear and tear' that apparently the chloroplast signalling system was not evolved to sense. In addition, the depletion of starch (glucose) during lincomycin treatment could have also contributed to the enhancement of expression of Lhcb genes as was reported earlier (Oswald *et al*. 2001; Pfannschmidt *et al*. 2001). Hence, finding ways to bypass the retrograde redox signalling could be a feasible approach to sustain plant growth in conditions of low RCs number and higher excitation pressure. Indeed, this strategy allowed the treated plants to have a similar leaf biomass compared with those untreated. It seems therefore that the physiology of the chloroplast retention of LHCII antenna at these conditions is a viable strategy that maintains light harvesting on standby in case the detrimental damage to the reaction centres will stop and the rejuvenation phase supplying the membrane with reaction centres will commence. Importantly, RCII seems to be able to consume the energy from a limited number of light-harvesting complexes (a puddle model) that is likely to be due to the limitation in the excitation energy propagation along the photosynthetic membrane (Belgio *et al*. 2012; van Amerongen & Croce 2013). This limitation also prevents large fluctuations in the energy influx into the RC and the building up of a large excitation pressure at the conditions of high light exposure.

ACKNOWLEDGMENTS

The authors thank Dr. Christopher Duffy and Prof. Conrad Mullineaux for critical reading of the manuscript; Dr. Giulia Mastroianni for helping with thin sections and electron microscopy; Prof. Dario Leister and Dr. Mathias Pribil for CURT1 protein antibody. This work was supported by The Leverhulme Trust and BBSRC research grants to A.V.R.

REFERENCES

Allen K.D., Duysen M.E. & Staehelin L.A. (1988) Biogenesis of thylakoid membranes is controlled by light intensity in the conditional chlorophyll b-deficient CD3 mutant of wheat. *The Journal of Cell Biology* **107,** 907–919.

Anderson J., Chow W.S. & De Las Rivas J. (2008) Dynamic flexibility in the structure and function of photosystem II in higher plant thylakoid membranes: the grana enigma. *Photosynthesis Research* **98,** 575–587.

Anderson J.M. & Osmond B. (2001) Sun-shade responses: compromises between acclimation and photoinhibition. In *Photoinhibition* (eds D.J. Kyle, B. Osmond & C.J. Arntzen), pp. 1–38. Elsevier, Amsterdam.

Anderson J.M., Chow W.S. & Goodchild D.J. (1988) Thylakoid membrane organisation in sun/shade acclimation. *Australian Journal of Plant Physiology* **15,** 11–26.

Armbruster U., Labs M., Pribil M., Viola S., Xu W., Scharfenberg M., . . . Leister D. (2013) Arabidopsis curvature thylakoid proteins modify thylakoid architecture by inducing membrane curvature. *The Plant Cell* **25,** 2661–2678.

Armond P.A., Staehelin L.A. & Arntzen C.J. (1977) Spatial relationship of photosystem I, photosystem II, and the light-harvesting complex in chloroplast membranes. *The Journal of Cell Biology* **73,** 400–418.

Arvidsson P.O. & Sundby C. (1999) A model for the topology of the chloroplast thylakoid membrane. *Australian Journal of Plant Physiology* **26,** 687–694.

Bachmann K.M., Ebbert V., Adams W.W. III, Verhoeven A.S., Logan B.A. & Demmig-Adams B. (2004) Effects of lincomycin on PSII efficiency, non-photochemical quenching, D1 protein and xanthophyll cycle during photoinhibition and recovery. *Functional Plant Biology* **31,** 803–813.

Baker N.R. & Bowyer J.R. (1994) *Photoinhibition of Photosynthesis: From Molecular Mechanisms to the Field*. Bios Scientific Publishers Ltd., Oxford.

Barber J. (1982) Influence of surface charges on thylakoid structure and function. *Annual Review of Plant Physiology* **33,** 261–295.

Barber J. (1995) Molecular-basis of the vulnerability of photosystem-II to damage by light. *Australian Journal of Plant Physiology* **22,** 201–208.

Bassi R. (1986) Studies on the leaf of *Trapa natans*: polymorphism of chloroplasts and microbodies. *Cytobios* **45,** 109–221.

Bassi R., Hinz U. & Barbato R. (1985) The role of the light harvesting complex and photosystem II in thylakoid stacking in the chlorina F2 barley mutant. *Carlsberg Research Communications* **50,** 347–367.

Belgio E., Johnson M.P., Jurić S. & Ruban A.V. (2012) Higher plant photosystem II light harvesting antenna, not the reaction center, determines the excited state lifetime – both the maximum and the non-photochemically quenched. *Biophysical Journal* **102,** 2761–2771.

Bennoun P., Spierer-Herz M., Erickson J., Girard-Bascou J., Pierre Y., Delosme M. & Rochaix J.D. (1986) Characterisation of photosystem II mutants of *Chlamydomonas reinhardii* lacking the psbA gene. *Plant Molecular Biology* **6,** 151–160.

Boekema E.J., Hankamer B., Bald D., Kruip J., Nield J., Boonstra A.F., . . . Rögner M. (1995) Supramolecular structure of the photosystem II complex from green plants and cyanobacteria. *Proceedings of the National Academy of Sciences of the United States of America* **92,** 175–179.

Bradford M.M. (1976) A rapid and sensitive method for the quantitation of microgram quantities of protein utilizing the principle of protein-dye binding. *Analytical Biochemistry* **72,** 248–254.

Caffarri S., Frigerio S., Olivieri E., Righetti P.G. & Bassi R. (2005) Differential accumulation of Lhcb gene products in thylakoid membranes of Zea mays plants grown under contrasting light and temperature conditions. *Proteomics* **5,** 758–768.

Chen Y.B., Durnford D.G., Koblizek M. & Falkowski P.G. (2004) Plastid regulation of Lhcb1 transcription in the chlorophyte alga *Dunaliella tertiolecta*. *Plant Physiology* **136,** 3737–3750.

Crouchman S., Ruban A.V. & Horton P. (2006) PsbS enhances nonphotochemical fluorescence quenching in the absence of zeaxanthin. *FEBS Letters* **580,** 2053–2058.

Denslow N.D. & O'Brien T.W. (1974) Susceptibility of 55S mitochondrial ribosomes to antibiotics inhibitory to prokaryotic ribosomes, lincomycin, chloramphenicol and PA114A. *Biochemical and Biophysical Research Communications* **57,** 9–16.

Drop B., Yadav K.N.S., Boekema E.J. & Croce R. (2014) Consequences of state transitions on the structural and functional organization of photosystem I in the green alga Chlamydomonas reinhardtii. *The Plant Journal* **78,** 181–191.

Duysen M.E., Freeman T.P., Williams N.D. & Huckle L.L. (1985) Chloramphenicol stimulation of light harvesting chlorophyll protein complex accumulation in a chlorophyll *b* deficient wheat mutant. *Plant Physiology* **78,** 531–536.

Eberhard S., Finazzi G. & Wollman F.-A. (2008) The dynamics of photosynthesis. *Annual Review of Genetics* **42,** 463–515.

Escoubas J.M., Lomas M., LaRoche J. & Falkowski P.G. (1995) Light intensity regulation of cab gene transcription is signaled by the redox state of the plastoquinone pool. *Proceedings of the National Academy of Sciences of the United States of America* **92,** 10237–10241.

Guiamet J.J., Tyystjarvi E., Tyystjarvi T., John I., Kairavuo M., Pichersky E. & Nooden L.D. (2002) Photoinhibition and loss of photosystem II reaction centre proteins during senescence of soybean leaves. Enhancement of photoinhibition by the 'stay-green' mutation cytG. *Physiologia Plantarum* **115,** 468–478.

Harrigan R.P., Hope M.J., Redelmeier T.E. & Cullis P.R. (1992) Determination of transmembrane pH gradients and membrane potentials in liposomes. *Biophysical Journal* **63,** 1336–1345.

Häusler R.E., Geimer S., Kunz H.H., Schmitz J., Dörmann P., Bell K., . . . Flügge U.-I. (2008) Chlororespiration and grana hyperstacking: how an Arabidopsis double mutant can survive despite defects in starch biosynthesis and daily carbon export from chloroplasts. *Plant Physiology* **149,** 515–533.

Holzwarth A.R., Miloslavina Y., Nilkens M. & Jahns P. (2009) Identification of two quenching sites active in the regulation of photosynthetic light-harvesting studied by time-resolved fluorescence. *Chemical Physics Letters* **483,** 262–267.

Iwai M., Yokono M., Inada N. & Minagawa J. (2010) Live-cell imaging of photosystem II antenna dissociation during state transitions. *Proceedings of the National Academy of Sciences* **107,** 2337–2342.

Jia H., Liggins J.R. & Chow W.S. (2012) Acclimation of leaves to low light produces large grana: the origin of the predominant attractive force at work. *Philosophical Transactions of the Royal Society of London. Series B, Biological Sciences* **367,** 3494–3502.

Johnson M.P., Goral T.K., Duffy C.D.P., Brain A.P.R., Mullineaux C.W. & Ruban A.V. (2011) Photoprotective energy dissipation involves the reorganization of photosystem II light harvesting complexes in the grana membranes of higher plant chloroplasts. *The Plant Cell* **23,** 1468–1479.

Kim E.H., Li X.P., Razeghifard R., Anderson J.M., Niyogi K.K., Pogson B.J. & Chow W.S. (2009) The multiple roles of light-harvesting chlorophyll a/b-protein complexes define structure and optimize function of Arabidopsis chloroplasts: a study using two chlorophyll b-less mutants. *Biochimica et Biophysica Acta* **1787,** 973–984.

Kiss A.Z., Ruban A.V. & Horton P. (2008) The PsbS protein controls the organization of the photosystem II antenna in higher plant thylakoid membranes. *The Journal of Biological Chemistry* **283,** 3972–3978.

Lee C.W., Antoniou-Kourounioti R., Chi-Sheng Wu J., Murchie E., Maroto-Valer M., Jensen O.E., . . . Ruban A.V. (2014) Photocatalytic conversion of CO_2 to hydrocarbons by light-harvesting complex assisted Rh-doped TiO_2 photocatalyst. *Journal of CO2 Utilisation* **5,** 33–40.

Livingston A.K., Cruz J.A., Kohzuma K., Dhingra A. & Kramer D.M. (2010) An Arabidopsis mutant with high cyclic electron flow around photosystem I (*hcef*) involving the NADPH dehydrogenase complex. *The Plant Cell* **22,** 221–233.

Miller K.R., Miller G.J. & McIntyre K.R. (1976) The light-harvesting chlorophyll-protein complex of photosystem II. Its location in the photosynthetic membrane. *The Journal of Cell Biology* **71,** 624–638.

Miloslavina Y., Wehner A., Lambrev P.H., Wientjes E., Reus M., Garab G., . . . Holzwarth A.R. (2008) Far-red fluorescence: a direct spectroscopic marker for LHCII oligomer formation in non-photochemical quenching. *FEBS Letters* **582,** 3625–3631.

Mullineaux C.W. (2005) Function and evolution of grana. *Trends in Plant Science* **10,** 521–525.

Mulo P., Pursiheimo S., Hou C.X., Tyystjärvi T. & Aro E.M. (2003) Multiple effects of antibiotics on chloroplast and nuclear gene expression. *Functional Plant Biology: FPB* **30,** 1097–1103.

Mustárdy L. & Garab G. (2003) Granum revisited. A three-dimensional model – where things fall into place. *Trends in Plant Science* **8,** 117–122.

Nacir H. & Bréhélin C. (2013) When proteomics reveals unsuspected roles: the plastoglobule example. *Frontiers in Plant Science* **4,** 1–8.

Nedukha O.M. (2012) Ultrastructural characteristic of cells and pigment analysis in floating and submerged leaves of *Trapa natans* L. *Modern Phytomorphology* **81,** 81–84.

Nevo R., Charuvi D., Tsabari O. & Reich Z. (2012) Composition, architecture and dynamics of the photosynthetic apparatus in higher plants. *The Plant Journal* **70,** 157–176.

Nooden L.D. (1988) The phenomena of senescence and aging. In *Senescence and Aging in Plants* (eds L.D. Nooden & A.C. Leopold), pp. 1–50. Academic Press, Inc., San Diego, CA, USA.

Nott A., Jung H.-S., Koussevitzky S. & Chory J. (2006) Plastid-to-nucleus retrograde signalling. *Annual Review of Plant Biology* **57,** 739–759.

Ögren E. (1994) The significance of photoinhibition for photosynthetic productivity. In *Photoinhibition of Photosynthesis: From Molecular Mechanisms to the Field* (eds N.R. Baker & J.R. Bowyer), pp. 433–448. Bios Scientific Publishers Ltd., Oxford.

Oswald O., Martin T., Dominy P.J. & Graham I.A. (2001) Plastid redox state and sugars: interactive regulators of nuclear-encoded photosynthetic gene expression. *Proceedings of the National Academy of Sciences of the United States of America* **98,** 2047–2052.

Petracek M.E., Dickey L.F., Huber S.C. & Thompson W.F. (1997) Light-regulated changes in abundance and polyribosome association of ferredoxin mRNA are dependent on photosynthesis. *The Plant Cell* **9,** 2291–2300.

Petrou K., Belgio E. & Ruban A.V. (2014) pH sensitivity of chlorophyll fluorescence quenching is determined by the state of LHCII aggregation. *Biochimica et Biophysica Acta* **1837,** 1533–1539.

Pfannschmidt T. (2003) Chloroplast redox signals: how photosynthesis controls its own genes. *Trends in Plant Science* **8,** 33–41.

Pfannschmidt T., Schutze K., Brost M. & Oelmüller R. (2001) A novel mechanism of nuclear photosynthesis gene regulation by redox signals from the chloroplast during photosystem stoichiometry adjustment. *The Journal of Biological Chemistry* **276,** 36125–36130.

Platt T., Gallegos C.L. & Harrison W.G. (1980) Photoinhibition of photosynthesis in natural assemblages of marine phytoplankton. *Journal of Marine Research* **38,** 687–701.

Porra R.J., Thompson W.A. & Kriedemann P.E. (1989) Determination of accurate extinction coefficients and simultaneous equations for assaying chlorophylls *a* and *b* extracted with four different solvents: verification of the concentration of chlorophyll standards by atomic absorption spectroscopy. *Biochimica et Biophysica Acta* **975,** 384–394.

Powles S.B. (1984) Photoinhibition of photosynthesis induced by visible-light. *Annual Review of Plant Physiology and Plant Molecular Biology* **35,** 15–44.

Ruban A. (2012) *The Photosynthetic Membrane: Molecular Mechanisms and Biophysics of Light Harvesting*. Wiley-Blackwell, Chichester.

Ruban A.V., Solovieva S., Lee P.J., Ilioaia C., Wentworth M., Ganeteg U., . . . Horton P. (2006) Plasticity in the composition of the light harvesting antenna of higher plants preserves structural integrity and biological function. *The Journal of Biological Chemistry* **281,** 14981–14990.

Ruban A.V., Johnson M.P. & Duffy C.D.P. (2012) The photoprotective molecular switch in photosystem II. *Biochimica et Biophysica Acta* **1817,** 167–181.

Shimoni E., Rav-Hon O., Ohad I., Brumfeld V. & Reichb Z. (2005) Three-dimensional organization of higher-plant chloroplast thylakoid membranes revealed by electron tomography. *The Plant Cell* **17,** 2580–2586.

Simpson D.J. (1979) Freeze-fracture studies on barley plastid membranes. III. Location of the light harvesting chlorophyll-protein. *Carlsberg Research Communications* **44,** 305–336.

Simpson D.J. (1982) Freeze-fracture studies on barley plastid membranes *V. viridis*-n34, a photosystem I mutant. *Carlsberg Research Communications* **47,** 215–225.

Simpson D.J., Vallon O. & von Wettstein D. (1989) Freeze-fracture studies on barley plastid membranes. VIII. In viridis-^{115}, a mutant completely lacking Photosystem II, oxygen evolution enhancer 1 (OEE1) and the a-subunit of cytochrome b-559 accumulate in appressed thylakoids. *Biochimica et Biophysica Acta* **975,** 164–174.

Staehelin L.A. (1976) Reversible particle movements associated with unstacking and restacking of chloroplast membranes in vitro. *The Journal of Cell Biology* **71,** 136–158.

Staehelin L.A. (2003) Chloroplast structure: from chlorophyll granules to supra-molecular architecture of thylakoid membranes. *Photosynthesis Research* **76,** 185–196.

Trissl H.W. & Wilhelm C. (1993) Why do thylakoid membrane from higher plants form grana stacks? *Trends in Biochemical Sciences* **18,** 415–419.

Ünlü C., Drop B., Croce R. & van Amerongen H. (2014) State transitions in *Chlamydomonas reinhardtii* strongly modulate the functional size of photosystem II but not of photosystem I. *Proceedings of the National Academy of Sciences* **111,** 3460–3465.

van Amerongen H. & Croce R. (2013) Light harvesting in photosystem II. *Photosynthesis Research* **116,** 251–263.

Vallon O., Wollman F. & Olive J. (1986) Lateral distribution of the main protein complexes of the photosynthetic apparatus in *Chlamydomonas reinhardtii* and in spinach: an immunocytochemical study using intact thylakoid membranes and a PSII enriched membrane preparation'. *Photobiochemistry and Photobiophysics* **12,** 203–220.

Ware M.A., Belgio E. & Ruban A.V. (2015) Photoprotective capacity of non-photochemical quenching in plants acclimated to different light intensities. *Photosynthesis Research* doi: 10.1007/s11120-015-0102-4.

Woessner J.P., Gillham N.W. & Boynton J.E. (1987) Chloroplast genes encoding subunits of the H+-ATPase complex of *Chlamydomonas reinhardtii* are rearranged compared to higher plants: sequence of the atpE gene and location of the atpF and atpI genes. *Plant Molecular Biology* **8,** 151–158.

Yang Y., Jankowiak R., Lin C., Pawlak K., Reus M., Holzwarth A.R. & Li J. (2014) Effect of the LHCII pigment–protein complex aggregation on photovoltaic properties of sensitized TiO_2 solar cells. *Physical Chemistry Chemical Physics* **16,** 20856–20865.

Received 10 November 2014; accepted for publication 23 February 2015

SUPPORTING INFORMATION

Additional Supporting Information may be found in the online version of this article at the publisher's web-site:

Figure S1. Senescence-like ultrastructural changes in treated leaves. Ultrathin section of treated leaves (F_v/F_m~0.2) showing (a) cytoplasmic membrane whorls typical of senescing cells at the stage of breakdown and (b, c) massive osmiophilic deposits between the cell wall and the plastid envelope indicated by an arrow.

Figure S2. Typical fluorescence trace of treated Arabidopsis leaf with F_v/F_m ~0.3. The point, at the end of the second illumination cycle, where NPQ value was calculated and employed in Fig. 7, is indicated by an asterisk.